metals

MDPI

Article

Simplified Elastoplastic Fatigue Correction Factor Analysis Approach Based on Minimum Conservative Margin

Xuejiao Shao, Juan Du, Xiaolong Fu, Furui Xiong *, Hui Li, Jun Tian, Xifeng Lu and Hai Xie

Science and Technology on Reactor System Design Technology Laboratory, Nuclear Power Institute of China, Chengdu 610213, China; shaoxuejiao@163.com (X.S.); xueshao407@gmail.com (J.D.); doudoulb@foxmail.com (X.F.); lhcnpi@163.com (H.L.); tianjunhi@gmail.com (J.T.); xifeng_lu@163.com (X.L.); kareemxh@gmail.com (H.X.)

* Correspondence: xfr90311@gmail.com; Tel.: +86-028-8590-8428

Abstract: ASME and RCC-M codes specify an elastoplastic fatigue analysis technique: a simplified elastoplastic fatigue analysis method based on linear elastic analysis. In this method, the elastic strain range is multiplied by the elastoplastic correction factor (K_e) to envelope the actual plastic strain range for fatigue evaluation. The ASME or RCC-M provide the K_e parameters of typical materials, such as austenitic stainless steel and low alloy steel. However, how can the parameters of the material not included in the codes be determined? Based on the existing material Z2CND18.12 (nitrogen control) in the codes and taking into account various sensitive factors, the minimum conservative margin of K_e for this material is calculated, and then the parameters of nonstandard materials are determined iteratively based on the conservative margin. The sensitive factors include the different structure model, load types, the loading control mode, temperature value and the material constitutive model. Based this approach, the K_e parameters of TA16 are determined and verified by the transient with drastic change in temperature and pressure. The results of the case show that the simplified elastoplastic fatigue analysis can envelope the results of cyclic plastic fatigue analysis. The minimum margin approach established in this paper can reasonably determine the K_e value of materials beyond the ASME and RCC-M codes.

Keywords: simplified elastoplastic fatigue; conservative margin; cyclic plastic correction factor; RCC-M codes

check for updates

Citation: Shao, X.; Du, J.; Fu, X.; Xiong, F.; Li, H.; Tian, J.; Lu, X.; Xie, H. Simplified Elastoplastic Fatigue Correction Factor Analysis Approach Based on Minimum Conservative Margin. *Metals* **2022**, *12*, 943. https://doi.org/10.3390/met12060943

Academic Editor: Alberto Campagnolo

Received: 28 April 2022
Accepted: 23 May 2022
Published: 30 May 2022

Publisher's Note: MDPI stays neutral with regard to jurisdictional claims in published maps and institutional affiliations.

Copyright: © 2022 by the authors. Licensee MDPI, Basel, Switzerland. This article is an open access article distributed under the terms and conditions of the Creative Commons Attribution (CC BY) license (https://creativecommons.org/licenses/by/4.0/).

1. Introduction

The simplified elastoplastic fatigue analysis method is mainly used in the fatigue calculation of nuclear codes ASME [1] and RCC-M [2]. The main purpose of this method is to simplify the calculation process, multiplying the elastic strain range by the elastoplastic correction factor K_e [3] to envelope the actual strain range. It is adopted to prevent fatigue and fracture failure of the components in actual operation [4–7]. Because the simplified elastoplastic fatigue analysis has the characteristic of high efficiency, it is widely used in engineering [8–10]. A number of K_e factors from nuclear and non-nuclear codes is also evaluated and briefly discussed in reference [11–13], and an alternative improved plasticity correction method is proposed. Different from the ASME code, for austenitic stainless steel, RCC-M and ASME Code Case N-779 [14] explicitly distinguish between stresses arising due to mechanical and thermal loads.

The ASME or RCC-M provide K_e expressions and parameters for typical materials, such as austenitic stainless steel and low alloy steel. For determining the K_e of new material, the experimental method is too expensive. Shao et al. [15–17] proposed a numerical determination approach of K_e, but it did not give the determination process of the minimum margin of materials in the codes in detail, including the influence of sensitive factors on K_e.

In this paper, a numerical calculation method for determining the K_e parameters of new materials is established, based on the K_e parameters of austenitic stainless steel

Z2CND18.12 (nitrogen control) given in the code, and taking into account various sensitive factors. Titanium alloy TA16, as a new material, needs to be used in equipment, but lacks K_e parameters. The uniaxial tension, cyclic strain and stress experiments of TA16 are conducted to establish the constitutive models. The K_e expression and parameters of TA16 are determined by the K_e numerical calculation method. Then, the new K_e parameters of TA16 are applied to the simplified fatigue assessment of the feedwater nozzle. By comparing the simplified elastoplastic fatigue analysis and cyclic-plastic fatigue analysis of the structure, it is found that the elastic strain is larger than the elastoplastic strain after K_e modification. The correctness and conservativeness of the K_e of TA16 are verified. Accordingly, a simplified elastoplastic fatigue analysis technology of titanium alloy material is developed.

2. Analysis Method of K_e

2.1. K_e in ASME and RCC-M

For the case of mechanical load, ASME [1] and RCC-M [2] calculate K_e according to the range of primary plus secondary stress S_e and allowable stress intensity S_m by the formulas as follows:

$$K_{e(mech)} = \begin{cases} 1.0 & for\ S_n \le 3S_m \\ 1.0 + \frac{(1-n)}{n(m-1)}\left(\frac{S_n}{3S_m} - 1\right) & for\ 3S_m < S_n < 3mS_m \\ 1/n & for\ S_n \ge 3mS_m \end{cases} \quad (1)$$

where n is the material hardening index, and m is the ratio when the value of $S_n/3S_m$ reaches the maximum. The values for m and n are given in ASME and RCC-M for low alloy steel, martensitic stainless steel, carbon steel, austenitic stainless steel, and nickel-chromium-iron alloy.

Different from the ASME, for austenitic stainless steel, RCC-M [2] adopts the following formula to calculate the elastoplastic correction factor under thermal load:

$$K_{e(therm)} = \max\left| \begin{matrix} 1.86\left\{1 - \frac{1}{1.66 + (S_n/S_m)}\right\} \\ 1 \end{matrix} \right. \quad (2)$$

$$S_P = K_{e(mech)} S_{P(mech)} + K_{e(ther)} S_{P(therm)} \quad (3)$$

$K_{e(RCCM)}$ can be obtained according to Equation (3), based the $S_{p(mech)}$ and $S_{p(therm)}$, where S_p is the range of total stresses. The RCC-M code provides the parameters for some typical materials, such as austenitic stainless steel, low alloy steel, and so on. It is known from Equations (1) and (2) that the value of $K_{e(mech)}$ is determined by parameters m and n, and the value of $K_{e(therm)}$ is determined by parameters 1.86 and 1.66, defined as A and B, respectively.

2.2. Numerical Method for Determining K_e Parameters

Because the same expression of $K_{e(mech)}$ is used in RCC-M and ASME codes, the expression of elastoplastic correction factor in RCC-M and ASME will also be assumed for the new material. The $K_{e(thermal)}$ will also adopt the same expression as that of RCC-M austenitic stainless steel. Once the values of A, B, m, and n of the new materials are determined, the K_e expression can be established.

The numerical method needs to consider the following factors for the K_e:

(1) Influence of material strength and constitutive model

The experimental error will affect the yield stress strength and the allowable stress. Equation (1) shows that K_e is related to S_m, so the fluctuation in the strength value will affect the determination of K_e.

Different constitutive models can be used in finite element elastoplastic calculation. The multilinear elastoplastic constitutive model and nonlinear follow-up harden-

ing Chaboche model are adopted. Table 1 shows the stress and strain relationship of Z2CND18.12 (nitrogen control) at different temperatures, which can be used in the multilinear elastoplastic constitutive model. These properties come from Section 3—Tom 1, subsection z-appendix A3.3s of the RCC-MRx code [18].

Table 1. Stress and strain relationship of Z2CND18.12 (nitrogen control) at different temperatures.

T = 20 °C		T = 100 °C		T = 200 °C		T = 250 °C		T = 300 °C		T = 350 °C	
ε	σ (MPa)	ε	σ (MPa)	ε	σ (MPa)	ε	σ (MPa)	ε	σ (MPa)	ε	σ (MPa)
0.0011	220	0.0009	175	0.0008	150	0.0008	138	0.0008	130	0.0008	127
0.0023	250	0.0016	190	0.0019	170	0.0019	160	0.0013	140	0.0012	133
0.0027	260	0.0019	200	0.0026	180	0.0027	170	0.0018	150	0.0016	140
0.0033	270	0.0024	210	0.0037	190	0.0039	180	0.0026	160	0.0024	150
0.0041	280	0.0031	220	0.0052	200	0.0057	190	0.0039	170	0.0036	160
0.0051	290	0.0041	230	0.0075	210	0.0085	200	0.0058	180	0.0055	170
0.0064	300	0.0074	250	0.0107	220	0.0103	205	0.0088	190	0.0085	180
0.0092	315	0.0100	260	0.0129	225	0.0125	210	0.0133	200	0.0131	190

(2) Load effect

(a) Load type: thermal load; mechanical load; mixed load (thermal load plus mechanical load)
(b) Loading control mode: stress control and displacement control
(c) Temperature: two typical temperatures (T = 30 °C and T = 350 °C)

In order to consider the influence of different load types, loading control mode, and temperature, the working condition parameters shown in Table 2 are set for the finite element calculation.

Table 2. Load type and peak load range of each model.

Model	Mechanical Load			Mixed Load	
	Temperature (°C)	Axial Pressure (MPa)	Axial Displacement (mm)	Temperature (°C)	Internal Pressure (MPa)
Model-I	30	40~180	0.2~10	-	-
	350	40~120	0.1~7		
Model-II	30	215~460	9.5~28	30~450	−20~31
	350	140~280	6.5~17		

(3) Geometry

According to Equation (1), it is necessary to make the calculated primary plus secondary stress range distributed in the interval of $3S_m$~$6S_m$, and some adjustment methods such as the stress distribution and load value are adopted.

As shown in Figure 1, by adjusting the relevant size parameters, the stress concentration of the model can be changed. For the notched sheet, R is notch radius, and the stress distribution at the notched sheet will change if the R value is adjusted. The Model-II is a typical nozzle, and L3 is the length of the thickness region. The L3 can control the curvature of geometrical discontinuities, so as to change the stress distribution.

Figure 2 shows the x-direction strain nephogram of the finite element calculation of the notched sheet. It can be seen from Figure 2 that the maximum x-direction strain is located at node 125 or 127 at the center of the notch, whether it is elastic analysis or elastoplastic analysis. The stress and strain values of these two nodes will be taken as the discussion object in the subsequent finite element calculation.

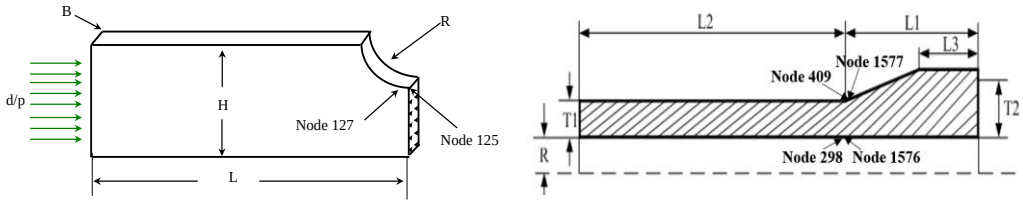

Figure 1. Notched sheet and nozzle finite element model.

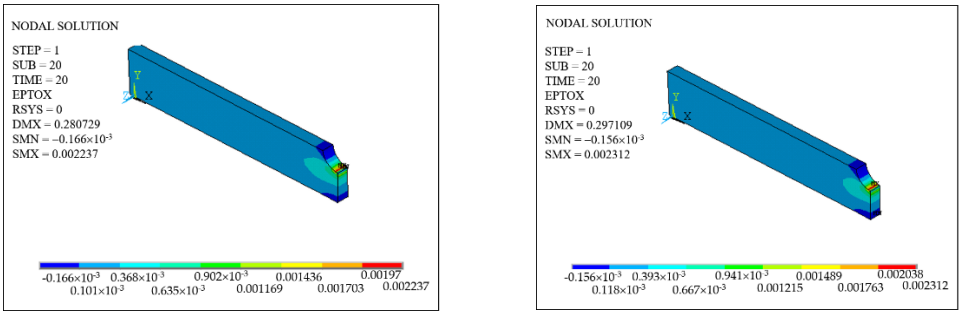

(**a**) (**b**)

Figure 2. Finite element simulated von Mises strain contour of notched sheet (X-direction, T = 20 °C, b = 20 mm, r = 25 mm, ratio = −1). (**a**) Elastic analysis; (**b**) elastoplastic analysis.

Figures 3 and 4 show the finite element calculation results of the nozzle under elastic analysis and elastoplastic analysis under the displacement control and load control, respectively. Among them, the load and displacement are applied at the right end. A pressure load and thermal load are applied to the inner surface of the nozzle together. It can be seen from the figures that the maximum deformation occurs at the transition section of node 409 and 298, marked in Figure 1, and the stress-strain of these nodes will be taken as the discussion object in the subsequent mechanical finite element calculation.

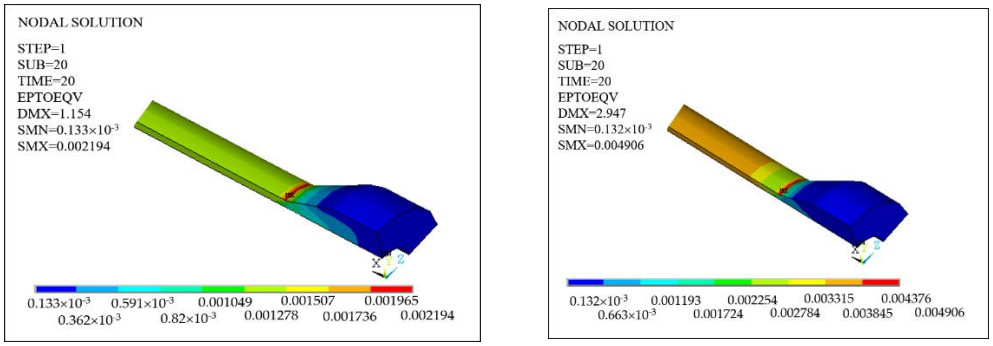

(**a**) (**b**)

Figure 3. Finite element simulated von Mises strain contour of nozzle under axial load. (**a**) Elastic analysis; (**b**) elastoplastic analysis.

(4) Loading waveform (Ratio)

A different ratio to control the loading waveform is selected (see Figure 5), such as in the four cases where the ratio is 0, −0.5, −0.8 and −1. The ratio is equal to the ratio of the minimum load to the maximum load during the cycle. Even under the same load, different results can be obtained by adjusting the ratio.

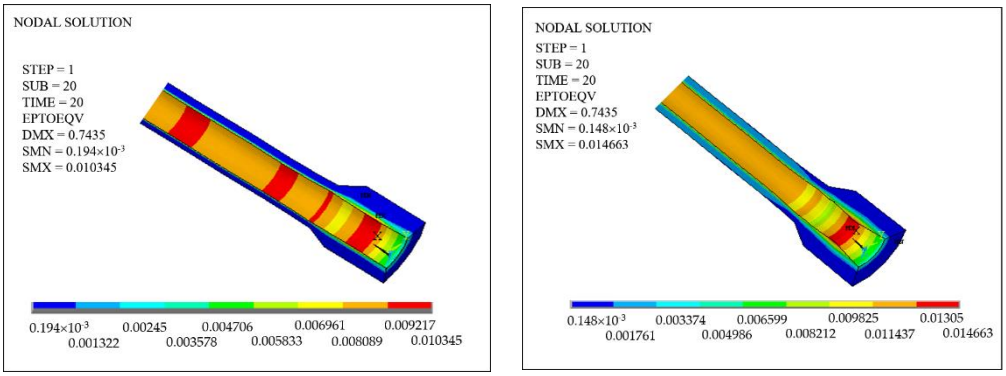

(**a**) (**b**)

Figure 4. Finite element simulated von Mises strain contour of nozzle under mechanical and thermal loads. (**a**) Elastic analysis; (**b**) elastoplastic analysis.

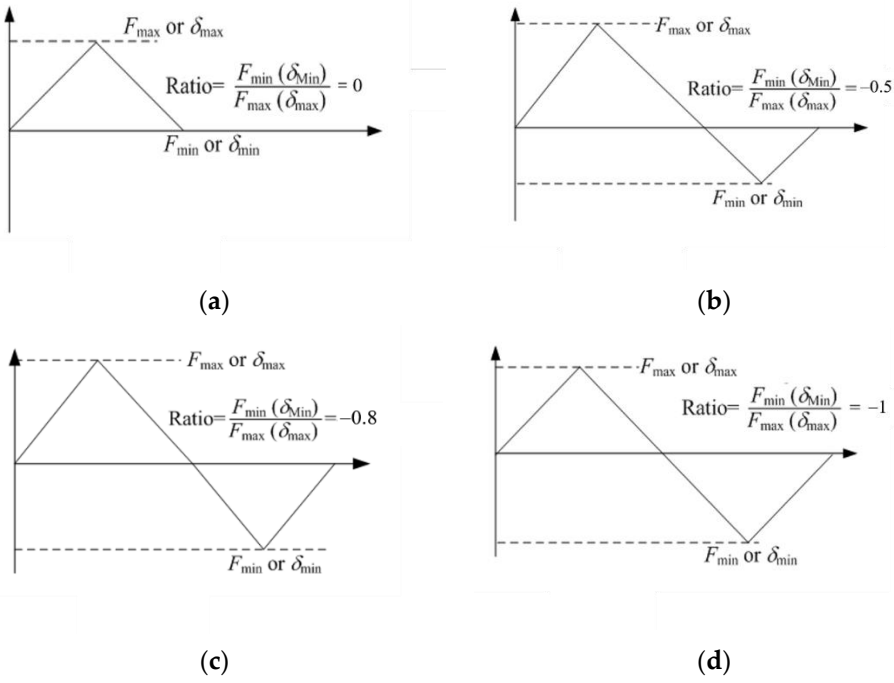

(**a**) (**b**)

(**c**) (**d**)

Figure 5. Loading waveforms under different ratios. (**a**) Ratio = 0; (**b**) Ratio = −0.5; (**c**) Ratio = −0.8; (**d**) Ratio = −1.

Figure 6 shows the stress-strain curves of different stress peak and valley ratios of 409 nodes simulated by the Chaboche model. It can be seen from the figure that the cyclic stress-strain curve is closely related to the ratio, that is, with the increase in ratio, the cyclic strain (strain rate) increases. However, no matter what the ratio is, the cyclic stress-strain curve is stable after a certain number of cycles (for example, when the number of cycles is 10, as shown in Figure 6c). Therefore, the number of cycles is controlled between 10 and 15 when the Chaboche model is used for finite element calculation later.

In this part, the notched sheet is taken as the representative to give detailed analysis results. Figure 7 shows the influence of the loading control mode on the elastoplastic correction factor at T = 20 °C and T = 350 °C, respectively. As shown in the figure:

(1) When T = 20 °C, there is little difference between the K_e calculated by the two loading control methods;

(2) When T = 350 °C, the calculated K_e of the load control loading mode is higher than that of the displacement control loading mode;

(3) The elastoplastic correction factors calculated under the two loading control modes are below the K_e (RCC-M).

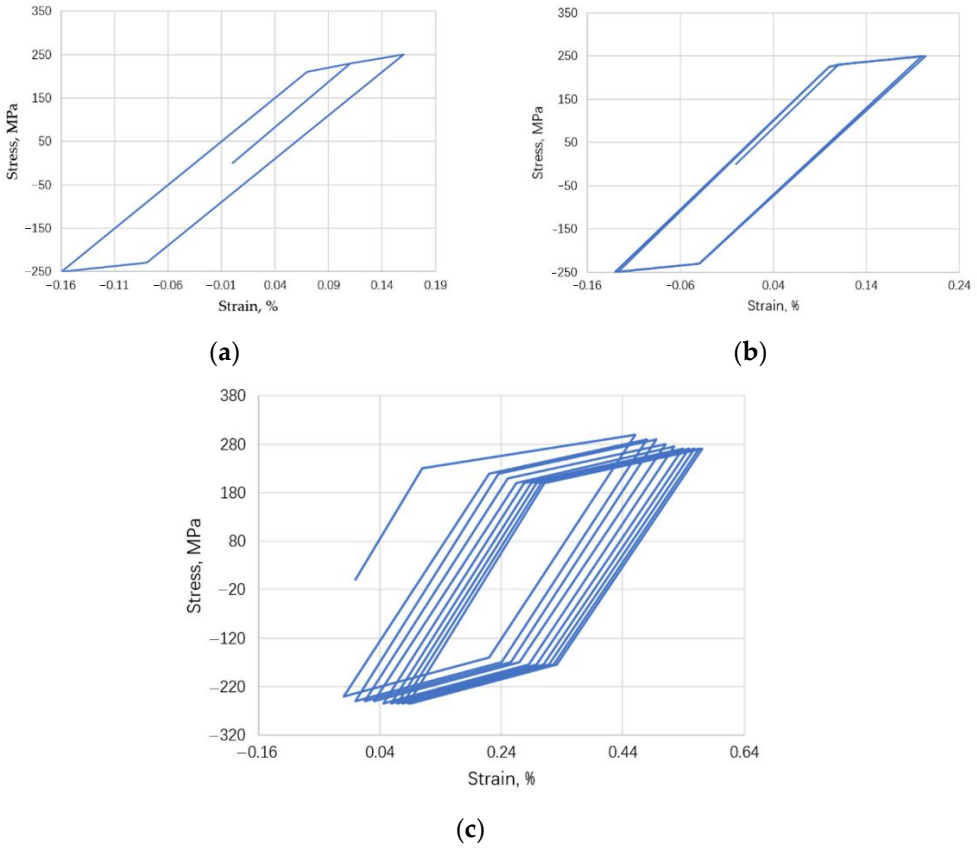

Figure 6. Stress-strain curves of 409 nodes in notched sheet simulated by Chaboche model under different ratios. (**a**) Ratio = −1; (**b**) ratio = −0.8; (**c**) ratio = −0.5.

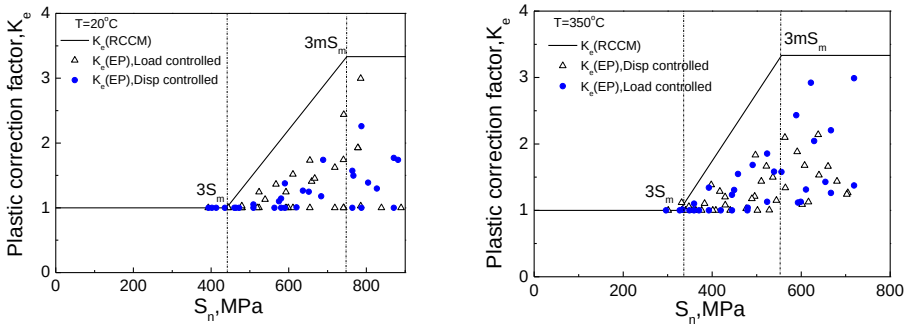

Figure 7. K_e with S_e under different loading control modes with notched sheet model.

Figure 8 shows the K_e with S_e calculated by the multilinear elastoplastic constitutive model and the nonlinear follow-up hardening model at T = 20 °C and T = 350 °C, respectively. It can be seen from the figure that under the two temperatures, the K_e calculated by the Chaboche model is significantly lower than that calculated by the EP model.

Figure 9 shows the K_e with S_e calculated at two temperatures (T = 20 °C and T = 350 °C). It can be seen from the figure that temperature is the key factor affecting the elastoplastic correction factor. Under the same S_e, the K_e value calculated at high temperature is much higher than that calculated at room temperature.

Based on the two typical structures, the effects of loading control mode, constitutive model, temperature, and load type on the elastoplastic correction factor K_e are calculated. The results of the nozzle model under thermal load are listed in Table 3. The results

show that the above factors affect the value of K_e, and $K_{e(EP)}$ is completely enveloped by K_e (RCC-M).

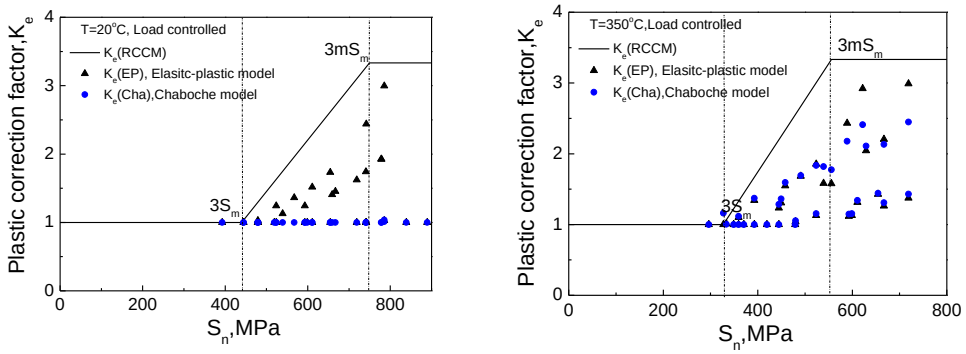

Figure 8. K_e with S_e under different constitutive models with notched sheet model.

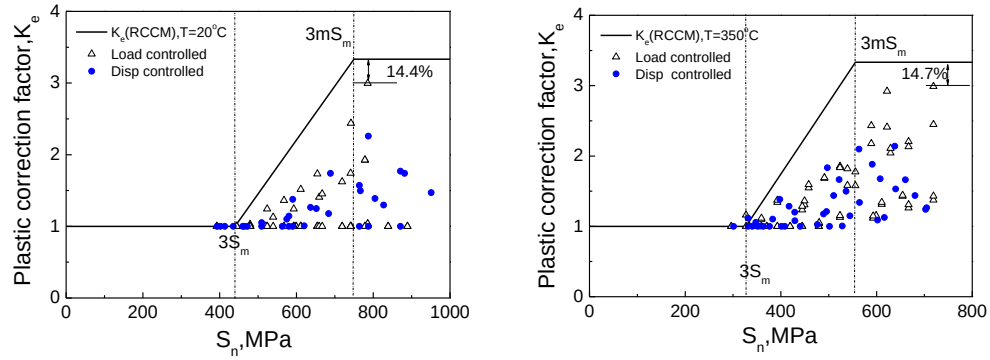

Figure 9. K_e with S_e under different temperatures with notched sheet model.

Table 3. Results of K_e under thermal load of Z2CND18.12 (nitrogen control) for nozzle model.

Node	Temp_Load (°C)	S_{n_th} (MPa)	$\Delta\varepsilon_{ee\_th}$ (%)	$\Delta\varepsilon_{ep\_th}$ (%)	K_{e_th} (EP)	K_{e_th} (RCCM)	η (%)
1576	350/20	693.23	6.276×10^{-3}	9.762×10^{-3}	1.555	1.628	11.580
	300/20	584.81	5.219×10^{-3}	7.835×10^{-3}	1.501	1.584	14.211
	250/20	476.68	4.190×10^{-3}	6.030×10^{-3}	1.439	1.528	16.819
	200/20	398.68	3.194×10^{-3}	4.373×10^{-3}	1.369	1.466	20.901
	125/20	212.00	1.800×10^{-3}	2.074×10^{-3}	1.152	1.260	41.625
298	350/20	748.98	6.368×10^{-3}	9.993×10^{-3}	1.569	1.642	11.331
	300/20	631.30	5.292×10^{-3}	8.071×10^{-3}	1.525	1.610	13.981
	250/20	514.53	4.251×10^{-3}	6.235×10^{-3}	1.467	1.568	17.905
	200/20	369.46	3.239×10^{-3}	4.486×10^{-3}	1.385	1.492	21.716
	125/20	228.73	1.825×10^{-3}	2.146×10^{-3}	1.176	1.365	51.851

Finally, the conservative margin of Z2CND18.12 (nitrogen control) under various sensitive factors can be determined as follows:

$$\eta = \min\left\{\frac{K_{e(RCCM)} - K_{e(EP)}}{K_{e(RCCM)} - 1}\right\}, \text{ when } S_n > 3mS_m \quad (4)$$

$K_{e(RCCM)}$ is obtained by Equations (1)–(3), and $K_{e(EP)}$ is obtained by dividing the elastoplastic strain range $\Delta\varepsilon_{ep}$ by the elastic strain range $\Delta\varepsilon_{ee}$. Based on a large number of calculations under various factors, Tables 3 and 4 give detailed calculation results of the condition where the minimum margin is located. It can be seen from Table 3 that the

minimum conservative margin of K_e under thermal load is 11.3%. The minimum conservative margin under mechanical load is 14.4% in Figure 9, and the minimum conservative margin under thermal mechanical coupling is 7.7% in Table 4. According to the previous description, the flowchart of the numerical method for determining the K_e parameters is shown in Figure 10.

Table 4. Results of K_e under thermal (ΔT = 280 °C) and pressure load of Z2CND18.12 (nitrogen control) for nozzle model.

Node	P (MPa)	S_n (MPa)	S_p (Therm)	S_p (Mech)	Δ_{ee} (%)	Δ_{ep} (%)	K_e (EP)	K_e (Therm)	K_e (Mech)	K_e (Mixed)	η (%)
1576	−30/0	609.5	1073.9	120.0	0.55	0.89	1.62	1.59	3.33	1.77	19.58
	−38/0	616.1	1073.9	152.0	0.56	0.93	1.66	1.59	3.33	1.81	17.96
	−60/0	646.0	1073.9	200.0	0.58	0.98	1.69	1.60	3.33	1.88	21.33
	−70/0	720.1	1073.9	280.0	0.61	1.08	1.76	1.63	3.33	1.98	22.20
	−80/0	775.7	1073.9	340.0	0.64	1.25	1.94	1.64	3.33	2.05	10.02
298	−30/0	655.0	1088.8	120.6	0.56	0.91	1.62	1.61	3.33	1.78	20.87
	−38/0	661.3	1088.8	152.7	0.56	0.94	1.67	1.61	3.33	1.82	18.96
	−60/0	675.4	1088.8	200.9	0.58	0.99	1.70	1.61	3.33	1.88	20.02
	−70/0	749.9	1088.8	281.3	0.62	1.10	1.78	1.63	3.33	1.98	20.75
	−85/0	805.9	1088.8	341.6	0.65	1.27	1.97	1.65	3.33	2.05	7.66

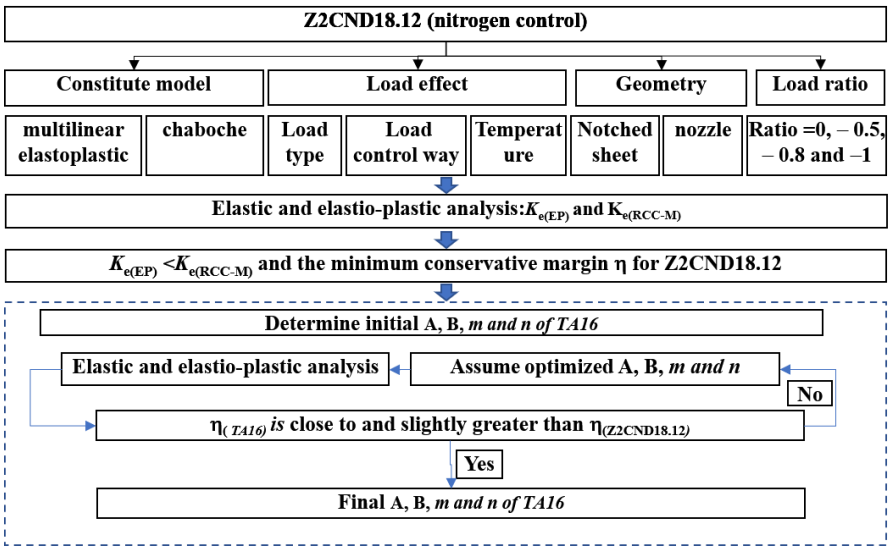

Figure 10. The flowchart of numerical method for determining K_e parameters.

3. Experiments and Constitutive Model

3.1. TA16 Axial and Cyclic Experiments

Firstly, the monotonic tension test, cyclic strain test, and stress test of TA16 [19] thin-walled circular tube at room and high temperatures are carried out. The chemical composition of TA16 is the same as in reference [20].

The monotonic tensile test adopts displacement control and the loading rate is 0.02 mm/s. The cyclic test is carried out under two control modes: strain control and stress control. The loading strain rate of the strain control is 0.2%/s, and the loading rate of the stress control is 100 MPa/s. The test equipment is MTS809. Figure 11 shows the uniaxial tensile stress-strain curves of TA16 at 30 °C and 350 °C. Figure 12a,c show the cyclic stress-strain curves of TA16 at different strain amplitudes at 30 °C and 350 °C, showing obvious cyclic stability characteristics. Figure 12b,d show the stable cyclic stress-strain curve of TA16. By comparison with the uniaxial tensile stress-strain curve, it is found that the uniaxial tensile curve of TA16 at 350 °C is slightly lower than that of the stable cyclic stress-strain curve.

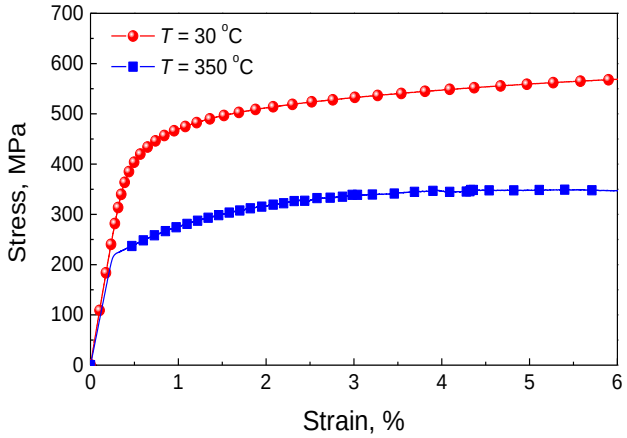

Figure 11. Uniaxial tensile stress-strain curves at 30 °C and 350 °C of TA16 titanium alloy.

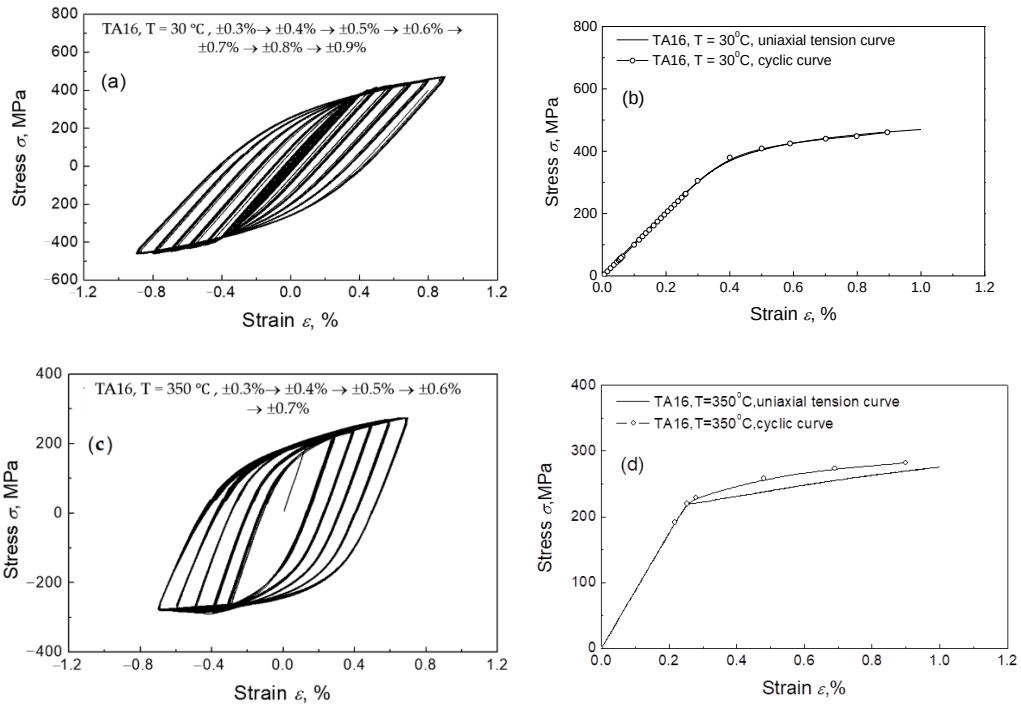

Figure 12. Experimental results under strain control: (**a**) cyclic stress-strain curve at room temperature; (**b**) stable cyclic curve and uniaxial tensile curve at room temperature; (**c**) cyclic stress-strain curves at 350 °C; (**d**) stable cyclic curve and uniaxial tensile curve at 350 °C.

Figure 13 shows the cyclic stress-strain curves of TA16 under stress control. It can be seen from these figures that TA16 has obvious ratcheting behavior. When TA16 is applied to the steam generator, it will bear a cyclic thermal load, which will inevitably lead to the production of ratcheting behavior. The cyclic accumulation of plastic strain occurs in the high stress region of the material, which will lead to structural deformation and damage, and then affect the service life of structures. Therefore, the ratcheting behavior must be reasonably considered in the structural design of titanium alloys.

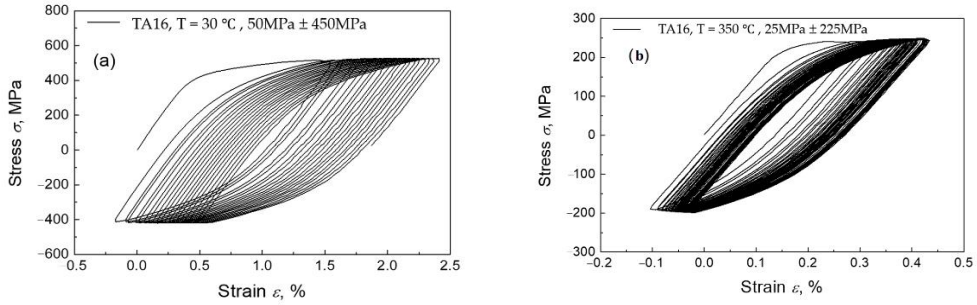

Figure 13. Cyclic stress-strain curve under stress control at room temperature (**a**) and 350 °C (**b**).

3.2. Cyclic Constitutive Model

The Chaboche constitutive model can describe the dynamic hardening and deformation behavior of materials in the stress-strain cycle; the back-stress evolution equation is as follows:

$$X = \sum_{i=1}^{M} X_i \tag{5}$$

$$\dot{X}_i = \frac{2}{3} C_i \dot{\varepsilon}^p - \gamma_i X_i \dot{p} \ (i = 1, 2) \tag{6}$$

The stress-strain curves under the strain control and stable cycling at different temperatures are fitted by the least square method. The parameters used in the Chaboche model are shown in Table 5, and the determination method of parameters can be found in [21].

Table 5. Material parameters of Chaboche model at different temperatures of TA16.

Temperature	c_1 (MPa)	γ_1	c_2 (MPa)	γ_2
30 °C	13,000	10	20,000	50
350 °C	20,000	5	1000	50

4. The K_e for New Material TA16

4.1. Determining K_e Parameters

Assuming the initial values of m and n for titanium alloy TA16, there are two suggestions for reference:

(1) In the RCC-M, the n value of low alloy steel, carbon steel, austenitic steel, and martensitic steel is 0.2~0.3 and the m value is 1.7~3.0.

(2) The value of m can be calculated according to when the elastic strain reaches 0.3%; n can be obtained by fitting the tensile stress-strain curve of the TA16 with the constitutive relationship $\sigma = A\varepsilon^n$.

According to the above principles, for titanium alloy TA16, the given initial value is m = 2.0 and n = 0.2. With reference to austenitic stainless steel, the initial values of A and B are A = 1.86 and B = 1.66, respectively.

The elastic and elastoplastic calculations under different loads are carried out by using the constitutive parameters of TA16 and considering the geometric model and load type in Section 2. The minimum conservative margin of TA16 under thermal load is 76.1%; under mechanical load, it is 64.7%; and under thermal mechanical coupling, it is 52.1%. These are much larger than the minimum conservative margin of austenitic stainless steel. It shows that the initial parameters are too conservative for calculating the elastoplastic correction factor of TA16, so the correlation coefficients A, B and m, n must be optimized.

The parameter values are adjusted repeatedly. Finally, the elastoplastic correction factor is recalculated to obtain the minimum conservative margin shown in Figure 14, which is close to and slightly greater than that of Z2CND18.12 (nitrogen control), indicating that the parameters of TA16 meet the requirements. Considering the fluctuation increase in TA16 material parameters, a conservative amount of 4.4% is added to the minimum

conservative margin of Z2CND18.12 (nitrogen control). The final values are A = 1.37, B = 1.26, m = 2.0 and n = 0.25.

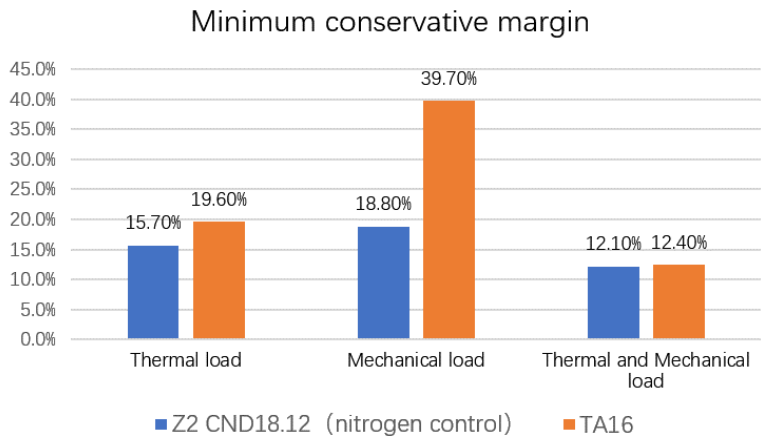

Figure 14. The minimum conservative margin of TA16 and Z2CND18.12 (nitrogen control).

4.2. Verification Calculation

Because of the drastic and frequent temperature transient of the steam generator, the stress exceeds the yield limit increases in some parts, such as the feed water nozzle. In this section, the feed water nozzle model is used to verify the conservativeness and correctness of the elastoplastic correction factor of TA16, and to realize the engineering application of the alloy elastoplastic correction factor. The transient temperature and pressure of the structure are calculated step by step. In the cyclic elastoplastic fatigue analysis, the transient combination with the greatest fatigue usage factor is selected.

The maximum principal strain range and the maximum alternating stress of the structure are calculated by the constitutive model in Section 1, and then the fatigue usage factor of the transient combination is obtained by using the fatigue curve. The simplified elastoplastic calculation results of nodes N1 and N2 under the combination of transients are shown in Table 6. The results of cyclic plastic fatigue analysis are shown in Table 7. From the comparison of the fatigue usage factor U in Tables 6 and 7, it can be seen that the fatigue usage factor of elastoplastic fatigue analysis is smaller than that of simplified elastoplastic analysis, and the elastoplastic correction factor calculated and optimized by the numerical analysis method can be reasonably applied to simplified elastoplastic fatigue analysis.

Table 6. Simulated results by simplified elastoplastic analysis.

Node	ΔP (MPa)	ΔT (°C)	S_n (MPa)	S_p (MPa)	S_m (MPa)	K_e	U_{max}
N1	0/16.6	84/279	329.1	428.2	234.9	2.20	0.66
N2	0/16.6	84/279	350.3	349.8	234.9	2.47	0.57

Table 7. Simulated results of cyclic elastoplastic fatigue analysis.

Node	Principal Strain Range	S_a (MPa)	N	n	U
N1	0.00516	280.3	400	100	0.25
N2	0.00434	235.9	555.6	100	0.18

Based on the determination of K_e for TA16 and the elastoplastic constitutive model, the simplified elastoplastic strain analysis technology is improved. The engineering application of K_e for TA16 is realized, which makes the analysis method provided by the code become implemented in structure design.

5. Conclusions

(1) Considering many kinds of sensitive factors, including different structure models, load types, loading control modes, temperature values and material constitutive models, the minimum conservative margin of K_e for Z2CND18.12 (nitrogen control) is 7.7%;
(2) According to the minimum conservative margin of Z2CND18.12 (nitrogen control), the elastic and elastoplastic calculations for TA16 are carried out, and the K_e of TA16 is determined as A = 1.37, B = 1.26, m = 2.0 and n = 0.25;
(3) For the feed water nozzle with dramatic temperature transient, the fatigue usage factor of the elastoplastic fatigue analysis is smaller than that of simplified elastoplastic analysis. It verifies the correctness and conservativeness of K_e for titanium alloy TA16.

Author Contributions: Methodology, J.T. and H.L.; supervision, X.F.; writing—original draft, X.S.; writing—review and editing, J.D. and F.X.; data curation, X.L.; validation, H.X. All authors have read and agreed to the published version of the manuscript.

Funding: This research was funded by the National Natural Science Foundation of China (12102416).

Institutional Review Board Statement: Not applicable.

Informed Consent Statement: Not applicable.

Data Availability Statement: Not applicable.

Conflicts of Interest: The authors declare no conflict of interest.

Nomenclature

A	The parameter of $K_{e(therm)}$
B	The parameter of $K_{e(therm)}$
C_i	Chaboche constitutive model parameter
K_e	Elastoplastic correction factor
m	The parameter of K_e
n	The material hardening index, K_e parameter
S_n	The range of primary plus secondary stress
S_p	The range of total stresses
S_m	The allowable stress intensity
γ_i	Chaboche constitutive model parameter
ε	Strain
$\dot{\varepsilon}^p$	Plastic strain rate
σ	Stress

References

1. ASME. *Asme Boiler and Pressure Vessel Code: Section III: Division 1 E Subsection Nb: Class 1 Components Rules for Construction of Nuclear Power Plant Components*; ASME: New York, NY, USA, 2010.
2. RCC-M. *Design and Construction Rules for Mechanical Components of PWR Nuclear Islands, Section I: Subsection B, Class 1 Components*; AFCEN: Paris, France, 2007.
3. Hubel, H. *Simplified Elasto-Plastic Fatigue Analysis of Smooth Structures*; European Commission: Madrid, Spain, 1995.
4. Branco, R.; Costa, J.; Borrego, L.; Berto, F.; Razavi, S.; Macek, W. Comparison of different one-parameter damage laws and local stress-strain approaches in multiaxial fatigue life assessment of notched components. *Int. J. Fatigue* **2021**, *151*, 106405. [CrossRef]
5. Cao, Y.; Nie, W.; Yu, J.; Tanaka, K. A novel method for failure analysis based on three-dimensional analysis of fracture surfaces. *Eng. Fail. Anal.* **2014**, *44*, 74–84. [CrossRef]
6. Kamal, M.; Rahman, M.M. Advances in fatigue life modeling: A review. *Renew. Sustain. Energy Rev.* **2018**, *82*, 940–949. [CrossRef]
7. Macek, W.; Branco, R.; Korpyś, M.; Łagoda, T. Fractal dimension for bending–torsion fatigue fracture characterisation. *Measurement* **2021**, *184*, 109910. [CrossRef]
8. Fu, X.; Wang, D. Plastic correction in simplified elasto-plastic fatigue analysis of nuclear components. *Mech. Eng.* **2017**, *1*, 67–70.
9. Zhang, J.; Li, W.; Dai, H.; Liu, N.; Lin, J. Study on the elasticoplastic correlation of low-cycle fatigue for variable asymmetric loadings. *Materials* **2020**, *13*, 2451. [CrossRef] [PubMed]
10. Fu, X.L.; Zhang, L.P.; Tian, J.; Shao, X.J.; Du, J.; Zhang, Y.; Liu, Z.Y. Plastic Strain Correction in Fatigue Analysis of Nuclear Power Plant Equipment. *Strength Mater.* **2021**, *53*, 183–188. [CrossRef]

11. Clarkson, D.M.; Bell, C.D.; Mackenzie, D. Critical review of ASME III plasticity correction factors for fatigue design-by-analysis of nuclear power plant components. *J. Press. Vessel. Technol.* **2021**, *143*, 061201. [CrossRef]
12. Lang, H.; Rudolph, J.; Ziegler, R. Performance study of Ke factors in simplified elastic plastic fatigue analyses with emphasis on thermal cyclic loading. *Int. J. Press. Vessel. Pip.* **2011**, *88*, 330–347. [CrossRef]
13. Slagis, G.C. Meaning of Ke in design-by-analysis fatigue evaluation. *J. Press. Vessel. Technol.* **2006**, *128*, 8–16. [CrossRef]
14. ASME. *ASME Boiler and Pressure Vessel Code, Case N-779: Alternative Rules for Simplified Elastic Plastic Analysis*; ASME: New York, NY, USA, 2010.
15. Shao, X.; Du, J.; Zhang, L.; Xie, H.; Tian, J.; Shi, K.; Zhang, Y.; Liu, Z. Determination method of elasto-plastic correction factor of TA16 titanium alloy based on RCC-M code methodology. *J. Press. Vessel. Technol.* **2021**, *143*, 88–93. [CrossRef]
16. Du, J.; Shao, X.; Zhang, L.; Kan, Q. Research on Elastoplastic Strain Correction Factor of Titanium Alloy. *Nucl. Power Eng.* **2014**, *35*, 101–105.
17. Kan, Q.H.; Guo, S.J.; Li, J.; Kang, G.Z.; Yan, W.Y. Numerical investigation on plastic strain correction factor in simplified elasto-plastic fatigue analysis. *Appl. Mech. Mater.* **2017**, *853*, 226–230. [CrossRef]
18. RCC-MRx. *Design and Construction Rules for Mechanical Components of Nuclear Installations: High Temperature, Research and Fusion Reactors*; AFCEN: Paris, France, 2018.
19. He, K.; Zhao, Y.; Dang, Y.; Wang, L.; Jiang, F. Fatigue Behavior of TA16 Tube with Surface Defect under High Cycle Loading. *Nucl. Power Eng.* **2016**, *37*, 48–51.
20. Luo, Q.; Wang, L.; Chen, X. Studies on the corrosion behavior of TA16 and TA17 titanium alloys in high temperature and high pressure water. *Qing Jinshu* **2012**, *2*, 56–59.
21. Shao, X.; Xie, H.; Xiong, F.; Shi, K.; Yu, X. Comparative study on the nonlinear calculation of ratcheting deformation using different constitutive model. In Proceedings of the ASME Pressure Vessels and Piping Conference, Virtual, Online, 3 August 2020; PVP2020-21182.